Energy & Environmental Science

PAPER

View Article Online
View Journal | View Issue

Cite this: *Energy Environ. Sci.*, 2017, **10**, 1820

Cu nanowires shelled with NiFe layered double hydroxide nanosheets as bifunctional electrocatalysts for overall water splitting†

Luo Yu,[ab] Haiqing Zhou,[b] Jingying Sun,[b] Fan Qin,[c] Fang Yu,[b] Jiming Bao,[c] Ying Yu,*[a] Shuo Chen*[b] and Zhifeng Ren*[b]

Received 7th June 2017,
Accepted 13th July 2017

DOI: 10.1039/c7ee01571b

rsc.li/ees

Developing highly active and low-cost electrocatalysts with superior durability for both the oxygen evolution reaction (OER) and hydrogen evolution reaction (HER) is a grand challenge to produce hydrogen by electrolysis of water. Here, we report on a facile and scalable approach to fabricate highly efficient three-dimensional (3D) bulk catalysts of core–shell nanostructures, in which few-layer NiFe layered double hydroxide (LDH) nanosheets are grown on Cu nanowire cores supported on Cu foams, toward overall water splitting. Remarkably, benefiting from the 3D hierarchical nanoarchitecture with large surface areas, fast electron transport, and open-channels for effective gas release, the resulting 3D self-standing catalysts exhibit outstanding OER activity as well as excellent HER performance in an alkaline medium. Using them as bifunctional catalysts for overall water splitting, a current density of 10 mA cm^{-2} was achieved at a voltage of 1.54 V, and 100 mA cm^{-2} at 1.69 V with excellent durability, which is much better than the benchmark of IrO_2(+)//Pt(−) electrodes. Our 3D core–shell electrocatalysts significantly advance the research towards large-scale practical water electrolysis.

Broader context

Hydrogen is a clean, efficient and renewable energy carrier. Electrochemical water splitting, in which two important half reactions, the hydrogen evolution reaction (HER) and oxygen evolution reaction (OER), are involved, is an environmentally-benign and economic route to generate H_2 on a large scale. At present, considerable efforts are being devoted to fabricating robust catalysts that are monofunctional for one of these two reactions, rather than bifunctional for both the HER and OER, so it remains a great challenge to catalyze both the HER and OER efficiently in a base medium. Thus, it is very interesting to develop a robust bifunctional catalyst that drives both the HER and OER with high efficiency simultaneously. In particular, to realize the commercialization of water splitting, high-current operation of the catalysts is more desirable. Here we develop a facile and scalable approach to fabricate a self-standing 3D core–shell Cu@NiFe LDH electrocatalyst for highly efficient overall water splitting. Benefiting from the smart structure, the catalyst not only exhibits outstanding OER performance, especially for high current densities, but also decent HER performance in an alkaline electrolyte, thus functioning as a versatile electrode for efficient overall water splitting.

Introduction

The excessive consumption of fossil fuels produces too much carbon dioxide, which necessitates searching for clean energy sources.[1] Hydrogen (H_2) has high energy density and is environmentally friendly, so it is an ideal alternative to fossil fuels.[2,3] Electrochemical water splitting for H_2 production is an appealing approach, in which two half reactions, the hydrogen evolution reaction (HER) and oxygen evolution reaction (OER), are involved.[4–6] However, both the HER and OER are inefficient, and due to the high activation barrier and the sluggish four proton-coupled electron transfer, OER is the major bottleneck of the overall water splitting.[7–10] Currently, the state-of-the-art OER catalysts are iridium dioxide (IrO_2) and ruthenium dioxide (RuO_2), which normally exhibit small onset potential, but their overpotential to reach the current density of 100 mA cm^{-2} is still very large, not to mention the current densities of 500 and 1000 mA cm^{-2} for practical large-scale water electrolysis. In addition, their high cost and low earth abundance further limit their practical applications.[11–15] Therefore, substantial efforts

[a] College of Physical Science and Technology, Central China Normal University, Wuhan 430079, China. E-mail: yuying01@mail.ccnu.edu.cn
[b] Department of Physics and TcSUH, University of Houston, Houston, TX 77204, USA. E-mail: schen34@uh.edu, zren@uh.edu
[c] Department of Electrical and Computer Engineering, University of Houston, Houston, TX 77204, USA

† Electronic supplementary information (ESI) available: Experimental details and results. See DOI: 10.1039/c7ee01571b

have been devoted to developing efficient and low-cost OER catalysts to replace the noble metal catalysts, leading to new catalysts better than RuO_2 and IrO_2.[16–18] However, most of them are good for the OER in an alkaline medium, but not good at all for the HER in the same electrolyte. Clearly, bifunctional catalysts for overall water splitting are necessary and have been reported, but the performance, especially for high current densities is not satisfactory for practical applications. Therefore, it is highly imperative to develop better bifunctional catalysts to make large-scale water splitting practical.

Two dimensional (2D) layered materials have attracted increasing interest in the field of catalysis and energy storage due to their novel structural features.[19–21] Layered double hydroxides (LDHs) are promising 2D layered materials because of their low cost, abundance, and ease of scale-up.[22–24] Benefiting from the unique layered structures, which are favorable for diffusion of water molecules and fast release of gaseous products, LDH-based materials have been studied for efficient OER as well as bifunctional catalysts for water splitting. For instance, Hou *et al.* reported cobalt selenide and NiFe LDH nanosheets (NSs) grown on exfoliated graphene foil as a 3D electrode for overall water splitting, which achieved a current density of 20 mA cm^{-2} at 1.71 V in a base electrolyte.[25] Subsequently, LDH-based catalysts including NiFe LDH/$NiCo_2O_4$[26] and NiFe LDH/$NiCo_2S_4$[27] have been fabricated for overall water splitting. However, the performance is still not good enough, and the voltage for a high current density (100 mA cm^{-2}) is still very high, which is far from the requirements of practical applications.[28,29] It has been proved that the active sites of layered materials are at the edges of the 2D materials, rather than the basal planes.[30,31] Therefore, it is coveted to grow LDH-based catalysts with abundant exposed edges. Recently, Jia *et al.* adopted an exfoliation method to fabricate single layered NiFe LDH NSs on defective graphene for overall water splitting.[32] Benefiting from the numerous exposed edges of single layered nanosheets and synergetic effects of the composites, this bifunctional catalyst can achieve a current density of 20 mA cm^{-2} at a voltage of 1.5 V, which is the best for overall water splitting to date. Regrettably, the exfoliation method is complicated and costly, which makes it unsuitable for practical application on a large scale. Besides, conductive substrates with a polymer binder to immobilize the active materials are required to prepare the electrodes, which further increases the cost.[33] Hence, developing an alternative approach to fabricate NiFe LDH with more active sites on the self-standing conductive skeletons for water splitting is of great significance.

Rational design of the electrode architecture is a powerful method to promote the ultimate catalytic activity. Particularly, 3D core–shell nanoarchitectures grown on conductive substrates are of great interest owning to their large surface areas, efficient electron transfer, and intimate access to the electrolyte.[34,35] Recently, Liu *et al.* reported a hierarchical core–shell catalyst of $CoMoO_4$@CoMoS supported on N-doped reduced graphene oxide toward efficient HER.[36] Feng *et al.* developed Co@FeOOH core–shell nanotube arrays supported on Ni foams as efficient self-standing 3D electrodes for the OER.[37] The inner Co metal cores served as highly conductive layers to provide reliable electron transmission, and overcame the poor electrical conductivity of FeOOH; thus the hybrid can lower the energy barriers of intermediates and promote the catalytic reactions. In comparison with Co metal cores, Cu nanowires (NWs) are much more conductive, cheaper, and easier to synthesize. We think a 3D structure of NiFe LDH NS shells on Cu NW cores (designated as Cu@NiFe LDH) supported on Cu foam should be highly favorable for overall water splitting. Furthermore, as illustrated in Fig. 1, we can see that these 3D core–shell Cu@NiFe LDH catalysts have better mechanical integrity since the Cu NWs are directly grown on the Cu foam, and the Cu NWs firmly grasp the shell of NiFe LDH NSs, ensuring good electronic transport. In addition, the NiFe LDH NSs are mostly vertically grown on the Cu NWs, leaving lots of exposed edges, and the ultrathin feature with few-layer nanosheets further offers more active sites. Clearly, the 3D core–shell nanostructures can provide large surface areas with increased exposure of active sites, efficient electron transport from the inner Cu NWs to the surrounding NiFe LDH NSs, and fast release of gaseous products. Consequently, this 3D core–shell catalyst should yield outstanding OER activity as well as excellent HER performance

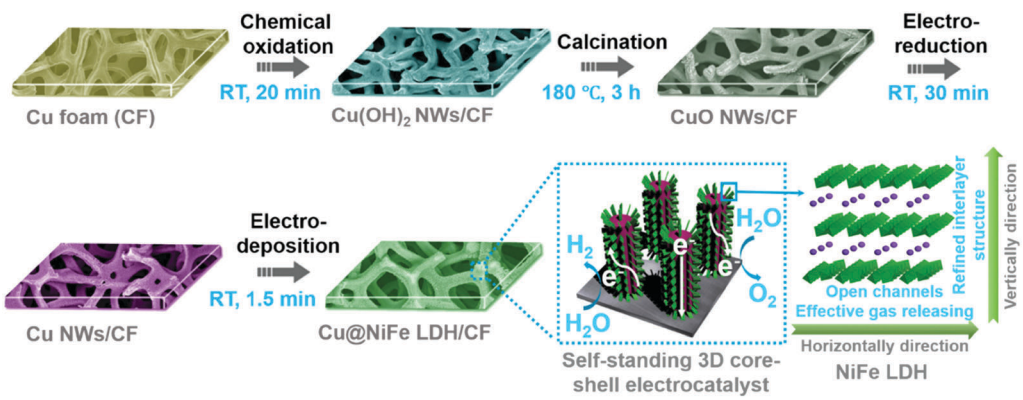

Fig. 1 Schematic illustration of the fabrication procedures of the self-standing 3D core–shell Cu@NiFe LDH electrocatalysts. (RT is the abbreviation for room temperature.)

in an alkaline medium, thus behaving as a bifunctional electrode for efficient overall water splitting.

Results and discussion

The fabrication process for the Cu@NiFe LDH core–shell composites is illustrated in Fig. 1. Cu foam was used as the substrate, and $Cu(OH)_2$ NWs were firstly synthesized through chemical oxidation of the Cu foam, which was followed by calcination in air to form CuO NWs. Cu NWs were obtained by electroreduction of CuO, which is a facile, safe, and low-cost approach compared with annealing in the presence of H_2. Finally, few-layer NiFe LDH NSs were electrodeposited on the Cu NWs, leading to the formation of the self-supported 3D core–shell Cu@NiFe LDH catalyst. It is worth mentioning that all the preparation steps were completed in a short time and at room temperature (except for the calcination), which led to low-cost. More importantly, the preparation steps are easy to scale up, a basic requirement for large-scale practical applications. Fig. S1 (ESI†) shows optical pictures of the as-prepared samples, displaying an apparent color change and uniformity during the process.

The morphology and core–shell nanostructure of the samples were revealed by scanning electron microscopy (SEM) and transmission electron microscopy (TEM). The SEM images of the Cu foam in Fig. S2 (ESI†) show its 3D porous structure with a smooth surface full of grain boundaries. Fig. S3 and S4 (ESI†) show SEM images of the $Cu(OH)_2$ NWs and CuO NWs, respectively. Both exhibit dense 1D structures and are roughly vertically on the substrate. Fig. 2a is the SEM image of the Cu@NiFe LDH at low magnification, which shows the 3D macroporous structure covered by uniform nanomaterials on the surface. Fig. 2b shows the SEM image of the Cu cores with a uniform 1D nanostructure. After electrodeposition, the NiFe LDH NSs uniformly and vertically grew on the Cu NWs, achieving a typical core–shell structure (Fig. 2c). The TEM image in Fig. 2d further shows that the nanosheets are interconnected with each other, forming a highly porous surface morphology, which offers many channels for electrolyte diffusion and gaseous product release. Fig. 2e displays a typical TEM image of an individual hybrid nanostructure, which distinctly exhibits that NiFe LDH NSs vertically grow on the Cu NWs, providing abundant exposed edges. The diameter of the core–shell hybrid is ~700 nm with an ~200 nm core of Cu NWs and ~250 nm shell of NiFe LDH NSs. Fig. 2f is a closer observation of the NiFe LDH NSs, in which the thickness of the NSs is determined to be ~3.2 to 4 nm. Since the thickness of a single layer of LDHs is about 0.8 nm,[38] the NiFe LDH NSs are around 4 to 5 layers for our samples. Such a 3D core–shell nanostructure with few-layer NiFe LDH NSs will maximize the surface area and enable more active edge sites to be exposed, thus promoting the catalytic activity. A distinctive lattice fringe with an interplanar spacing of 0.25 nm (inset in Fig. 2f) was also identified, which can be assigned to the (012) plane of NiFe LDH.[25] Energy dispersive X-ray spectroscopy (EDS) line scanning results (Fig. 2g) and EDS mapping analysis (Fig. 2h) further identify the quintessential core–shell structure, which clearly shows that copper is in the central part while both nickel and iron are homogeneously distributed throughout the whole composites. Pure NiFe LDH was also synthesized on the Cu foam by the same method for comparison, and the SEM images are displayed in Fig. S5 (ESI†), which shows that ultrathin and uniform NiFe LDH platelets compactly grow on the substrate.

We then carried out X-ray diffraction (XRD) measurements to identify the phase of the samples. As shown in Fig. 3a, three strong peaks located at 43.34°, 50.48°, and 74.17° all correspond to the cubic-structured Cu (PDF#65-9026). No peaks assigned to CuO or Cu_2O are found for the Cu NWs, meaning

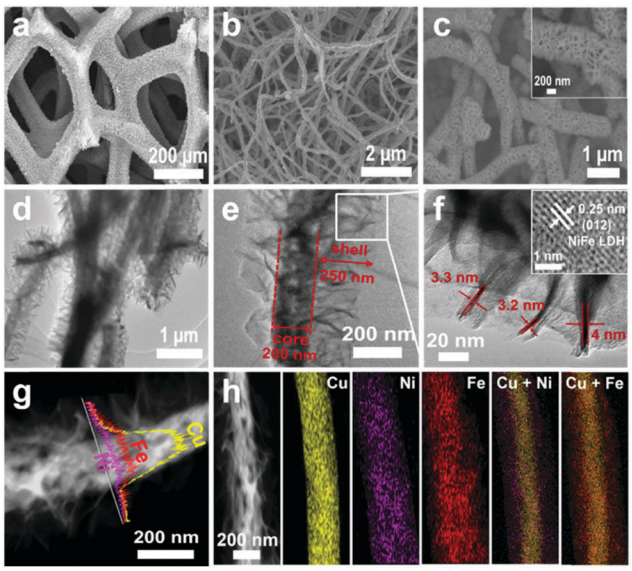

Fig. 2 Morphology and structure characterizations. SEM images of Cu@NiFe LDH at (a) low and (c) high magnification. (b) SEM image of Cu NWs. (d and e) TEM images of Cu@NiFe LDH. (f) Detailed image of the squared part in (e) and HRTEM image of Cu@NiFe LDH to show the lattice fringe (inset). (g) EDS line scan results, and (h) DF-STEM image of Cu@NiFe LDH with the corresponding elemental mapping.

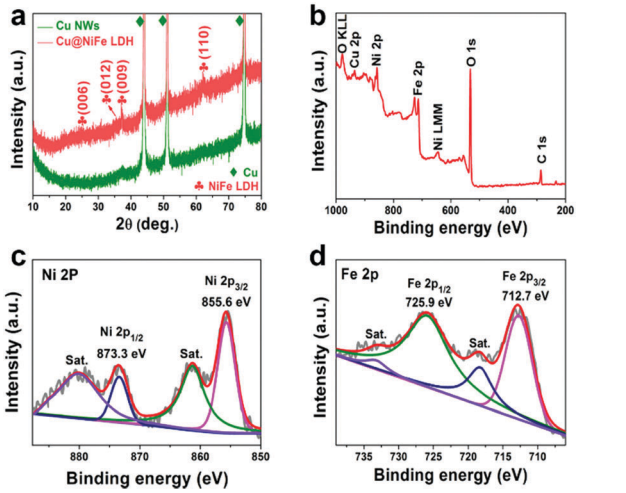

Fig. 3 (a) XRD patterns of Cu NWs and Cu@NiFe LDH. (b) XPS full spectrum, and high-resolution XPS spectra of (c) Ni 2p, and (d) Fe 2p for Cu@NiFe LDH.

the successful transformation from CuO to Cu. After electrodepositon of NiFe LDH, four small peaks show up on the XRD pattern of the composites, all of which are indexed to the LDHs.[39] X-ray photoelectron spectroscopy (XPS) measurements were further performed to probe the elemental composition and chemical valence states of the Cu@NiFe LDH. As shown in Fig. 3b, the full spectrum demonstrates the presence of Cu, Ni, Fe, O, and C (for calibration) elements in the composites. Fig. 3c and d are the high-resolution XPS spectra of Ni 2p and Fe 2p, respectively. In Fig. 3c, the two peaks located at binding energies of 855.6 and 873.3 eV correspond to Ni $2p_{3/2}$ and Ni $2p_{1/2}$, respectively,[27] along with two satellite peaks. For the XPS spectra of Fe 2p (Fig. 3d), two prominent peaks located at 712.7 and 725.9 eV are assigned to Fe $2p_{3/2}$ and Fe $2p_{1/2}$, respectively,[40] and two satellite peaks are located at 718.3 and 733.4 eV. All these features indicate that the Ni and Fe are present in the form of Ni^{2+} and Fe^{3+} oxidation states in the composites.[25]

The OER activity of the 3D core–shell electrode along with the pure NiFe LDH and commercial IrO_2 (on the Cu foam) was firstly assessed in 1 M KOH aqueous electrolyte using a standard three-electrode system. The polarization curves in Fig. 4a show that the Cu@NiFe LDH exhibits a much higher activity than the pure NiFe LDH and commercial IrO_2. Specifically, this 3D core–shell electrode can yield current densities of 10 and 100 mA cm^{-2} at overpotentials of 199 and 281 mV, respectively. In contrast, 233 and 307 mV overpotentials are required for the pure NiFe LDH, and 219 and 375 mV for the state-of-the art IrO_2 electrode to achieve the corresponding current densities. The OER performance of the Cu NWs and bare Cu foam is displayed in Fig. S6 (ESI†), and the activities are much worse than the pure NiFe LDH. For commercial applications, we also investigated the performance of high current densities. We found that a very small overpotential of 311 mV can drive a high current density of 500 mA cm^{-2}, and 315 mV for 1000 mA cm^{-2} for the Cu@NiFe LDH electrode, which is extremely superior to the pure NiFe LDH and IrO_2 catalysts. The Cu@NiFe LDH electrode also shows a very small Tafel slope of 27.8 mV dec^{-1} among the three catalysts (Fig. 4b), representing the inherent excellent OER activity. These results strongly demonstrate that our 3D core–shell Cu@NiFe LDH electrode is a highly efficient OER catalyst, especially for high current densities, which is much better than any reported data except for that reported by Zhou *et al.*,[48] as compared in Fig. 4c and Table S1 (ESI†). Additionally, the OER activity of Cu@NiFe LDH with different electrodeposition time of NiFe LDH was also studied and shown in Fig. S7 (ESI†); Cu@NiFe LDH-90 (the one labeled as Cu@NiFe LDH in the text) is better than Cu@NiFe LDH-60 and Cu@NiFe LDH-120. Notably, the Cu@NiFe LDH electrode exhibits remarkable durability as well during the OER test. As shown in Fig. 4d, the overpotentials to achieve current densities of 10 and 100 mA cm^{-2} do not seem to increase at all after 48 hours, which makes our samples very promising for large-scale commercial utilization. It is worth pointing out that the slight variation observed in Fig. 4d is reasonable, since the long-time stability test is a dynamic process, and many factors including bubble absorption on the surface of the electrodes will lead to slight potential variations.

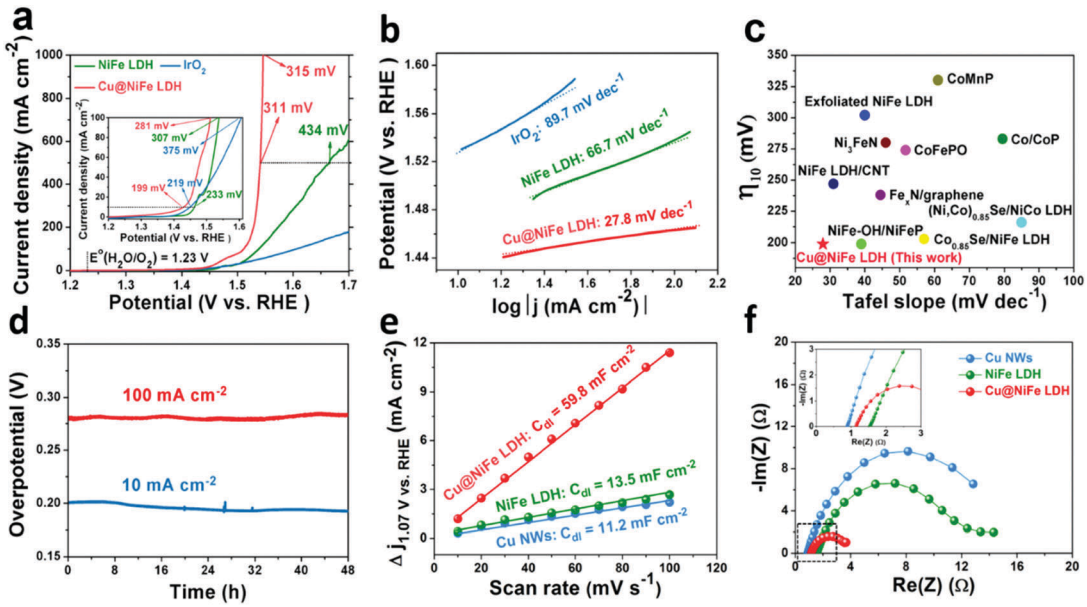

Fig. 4 OER performance of Cu@NiFe LDH conducted in 1 M KOH. (a) Polarization curves, and (b) corresponding Tafel plots. (c) Comparison of overpotential required at 10 mA cm^{-2} (η_{10}) and Tafel slope with other recently reported high-performance OER electrocatalysts. (d) Chronopotentiometry curves of Cu@NiFe LDH at constant current densities of 10 and 100 mA cm^{-2}. (e) Capacitive currents as a function of scan rate, and (f) Nyquist plots (overpotential = 250 mV) for the samples. The inset in (f) is the enlarged EIS curves of the squared parts. References cited in panel (c): NiFe-OH/NiFeP,[11] $Co_{0.85}$Se/NiFe LDH,[25] $(Ni,Co)_{0.85}$Se/NiCo LDH,[41] NiFe LDH/CNT (carbon nanotube),[42] Fe_xN/graphene,[43] Ni_3FeN,[44] CoFePO,[45] Co/CoP,[46] exfoliated NiFe LDH,[38] and CoMnP.[47]

In order to elucidate the possible origins of such extraordinary performance, we carried out cyclic voltammetry (CV) measurements to determine the double-layer capacitance (C_{dl}), which is proportional to the electrochemically active surface area (ECSA).[11,43] Fig. 4e shows the capacitive currents as a function of the scan rate obtained from the corresponding CV curves (Fig. S8, ESI†) to calculate C_{dl} for the electrodes. The Cu@NiFe LDH electrode possesses the highest C_{dl} of 59.8 mF cm^{-2}, which is nearly 4.5 and 5.5 times that of the pure NiFe LDH (13.5 mF cm^{-2}) and Cu NWs (11.2 mF cm^{-2}), respectively, demonstrating the improved ECSA and greater exposure of active sites achieved by the rational design of the 3D core–shell nanoarchitectures. The large ECSA is beneficial to water molecule adsorption and intimate contact with the electrolyte, along with rich active sites for catalytic reactions, which definitely account for the intensified activity. Meanwhile, electrochemical impedance spectroscopy (EIS) was utilized to study the electrode kinetics of the catalysts. As shown in Fig. 4f, the Cu@NiFe LDH electrode possesses a much smaller charge transfer resistance (R_{ct}) of ~2.8 Ω, in contrast to the pure NiFe LDH (12 Ω) and Cu NWs (15 Ω). The small R_{ct} reveals desirable electron transport and catalytic kinetics, leading to a small Tafel slope. In addition, the inset in Fig. 4f shows the enlarged EIS curves of the small resistance region, which exhibit that the Cu NWs and Cu@NiFe LDH electrodes have smaller series resistances (R_s), suggesting good electrical contacts with the substrate.[30] This is because that the Cu NWs are formed *via* direct reactions of Cu foam, leading to stronger adhesion to the substrate. And the Cu NWs firmly grasp the NiFe LDH NS shell, ensuring good electrical contacts and mechanical stability for the composites, which contribute to the superior stability as well.

To inspect the possibility of our 3D core–shell Cu@NiFe LDH catalysts for overall water splitting, we further evaluated the HER activity of the hybrid electrode in 1 M KOH. Surprisingly, the Cu@NiFe LDH catalysts also showed decent HER activity in the alkaline medium (Fig. 5a), which is much better than the pure NiFe LDH, Cu NWs, and Cu foam (Fig. S9, ESI†). It resulted in overpotentials of 116 and 192 mV to achieve current densities of 10 and 100 mA cm^{-2}, respectively. Although they are inferior to the commercial Pt wires, they are comparable to the NiMo alloy catalyst (synthesized on the Cu foam, Fig. S10, ESI†), which is reported to be a highly efficient HER catalyst in alkaline media.[49,50] Recently, Chen *et al.* pointed out that Pt may dissolve in the electrolyte, leading to the redeposition on the working electrode when using Pt as the counter electrode (CE), which significantly contributed to the HER activity.[51] Therefore, we further took a graphite rod as the CE to inspect the HER activity of our catalyst in the same conditions. As shown in Fig. S11 (ESI†), the polarization curve is almost the same as that of using Pt as the CE, eliminating the concern of Pt dissolution in our system. The Tafel slope of the Cu@NiFe LDH electrode is calculated to be 58.9 mV dec^{-1} (Fig. 5b), which is smaller than that of the pure NiFe LDH. In addition, as shown in Fig. 5c, the hybrid electrode is also very stable during the HER in 1 M KOH. Table S2 (ESI†) presents a detailed comparison of the HER performance for Cu@NiFe LDH with other recently reported

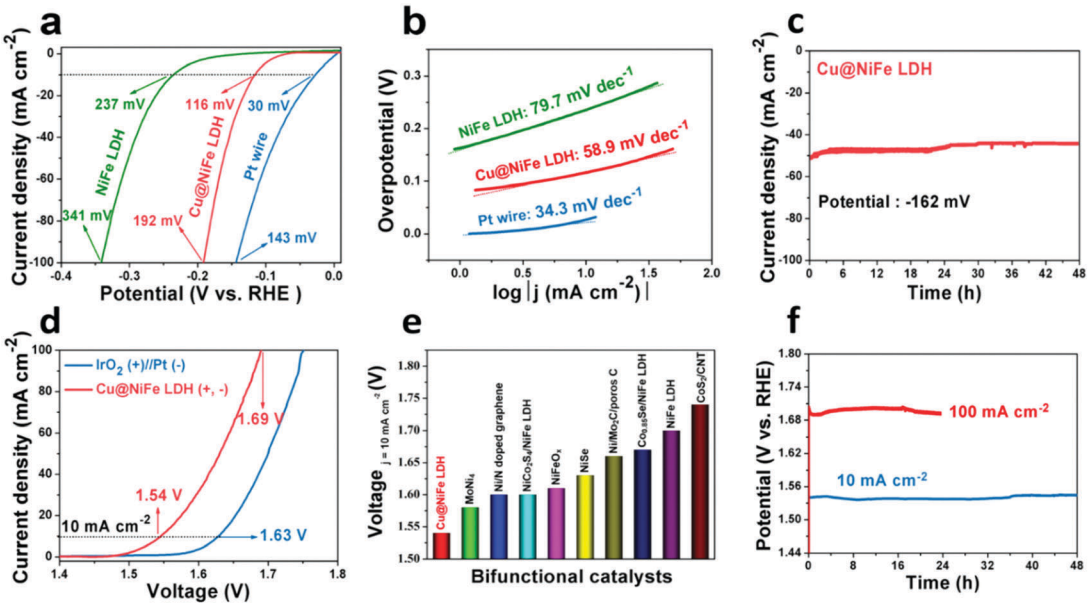

Fig. 5 HER and overall water splitting performance of Cu@NiFe LDH conducted in 1 M KOH. (a) HER polarization curves, and (b) corresponding Tafel plots of the electrodes. (c) Time dependence of the current density for Cu@NiFe LDH under a constant overpotential of 162 mV to afford a current density of 50 mA cm^{-2}. (d) Polarization curves for overall water splitting with the Cu@NiFe LDH electrode as both the anode and cathode at a scan rate of 2 mV s^{-1}. (The benchmark electrodes of IrO_2(+)//Pt(−) are tested the same way.) (e) Comparison of the required voltage at a current density of 10 mA cm^{-2} for the Cu@NiFeLDH catalyst in this work with other state-of-the-art noble metal free bifunctional catalysts. (f) Chronopotentiometry curves of Cu@NiFe LDH at a constant current density of 10 and 100 mA cm^{-2} tested in a two-electrode configuration. References cited in panel (e): $MoNi_4$,[57] Ni/N doped graphene,[58] $NiCo_2S_4$/NiFe LDH,[27] $NiFeO_x$,[59] NiSe,[60] Ni/Mo_2C/porous C,[61] $Co_{0.85}Se$/NiFe LDH,[25] NiFe LDH,[62] and $CoSe_2$/CNT (carbon nanotube).[33]

catalysts in alkaline electrolytes, showing that our self-standing 3D core–shell catalyst is better than most of the non-noble metal-based HER catalysts in base even though much better performances have been reported for many catalysts for the HER in acid.[2,30,52–56]

Both the outstanding OER activity and the encouraging HER activity of the Cu@NiFe LDH in the alkaline electrolyte inspired us to evaluate the overall water splitting performance by using the Cu@NiFe LDH electrode as both the anode and cathode in a two-electrode system. As shown in Fig. 5d, the Cu@NiFe LDH electrodes can achieve a current density of 10 mA cm^{-2} at a voltage of 1.54 V, and 100 mA cm^{-2} at 1.69 V, which are better than the benchmark of IrO_2(+)//Pt(−) electrodes. Notably, the voltage of IrO_2(+)//Pt(−) at 10 mA cm^{-2} (1.63 V) is larger than the overpotential sums of IrO_2 for OER and Pt for HER, and we attribute the difference to the poor stability of IrO_2 and flaccid attachment between IrO_2 and Cu foam (see discussion details in the ESI†). The performance at the current density of 10 mA cm^{-2} also outperforms most non-noble metal bifunctional catalysts for overall alkaline water splitting (Fig. 5e and Table S3, ESI†). Impressively, to afford higher current densities of 200, 300, and 500 mA cm^{-2}, the Cu@NiFe LDH electrodes just require voltages of 1.78, 1.85, and 1.99 V (Fig. S12, ESI†). This performance at higher current densities is even better than the aforementioned catalyst of exfoliated NiFe LDH/defective graphene, which sets a record of 20 mA cm^{-2} by a voltage of 1.5 V for overall water splitting.[32] At the same time, the Cu@NiFe LDH electrodes exhibit very good stability upon long-term testing both at current densities of 10 and 100 mA cm^{-2} (Fig. 5f). Moreover, a battery with a voltage of 1.5 V can drive overall water splitting with obvious gas bubble release, confirming the high efficiency of the Cu@NiFe LDH electrodes (Fig. S13, ESI†). Finally, we used gas chromatography to detect the gaseous products from the overall water splitting by the Cu@NiFe LDH electrodes. As shown in Fig. S14 (ESI†), H_2 and O_2 with a predicted ratio of 2 : 1 are detected, and the amount of measured H_2 and O_2 matches well with the calculated results, indicating a nearly 100% Faradaic efficiency. The outstanding catalytic activity of the Cu@NiFe LDH could be attributed to the following factors: (1) the Cu NWs rooted into the Cu foam firmly grasp the shell NiFe LDH NSs, not only ensuring good electrical contacts and mechanical stability, but also avoiding the use of extra binders. (2) The few-layer NiFe LDH NSs vertically grow on the Cu NWs, leaving abundant exposed edges, which offers more active sites for catalytic reactions. (3) The layered structure of NiFe LDH is favorable for diffusion of water molecules, ensuring intimate contact between the catalyst and electrolyte. And the interlayer spacing is propitious to gaseous product release. (4) The unique 3D core–shell structures can provide large surface areas with increased exposure of active sites and rapid release of gaseous products. Also, it facilitates the efficient electron transfer from the inner metallic Cu NWs to the outer shell of the NiFe LDH layer.

Lastly, the morphology and composition of the Cu@NiFe LDH catalyst on the anode and cathode sides after stability test for 24 h were examined. Fig. S15 (ESI†) shows the SEM images of Cu@NiFe LDH after the OER stability test, which retains the previous 3D porous structure with a little aggregation. The TEM image in Fig. 6a reveals that the core–shell nanostructure of Cu NWs and NiFe LDH NSs is well preserved. Moreover, the interplanar spacing of 0.25 nm corresponding to the (012) plane of NiFe LDH is still observed (Fig. 6b) after the OER stability test. The EDS mapping images in Fig. 6c further confirm the intact core–shell structure with a homogeneous distribution of the elements. Fig. S16 (ESI†) shows the same situation for the cathode (HER) after the stability test. The XRD pattern of the Cu@NiFe LDH catalysts after the stability test (Fig. S17a, ESI†) also matches well with the initial one, indicating no phase change of NiFe LDH after OER and HER tests. In Fig. 6d and e, the high-resolution XPS spectra of Ni 2p and Fe 2p, along with the full spectra in Fig. S17b (ESI†) of the Cu@NiFe LDH after the OER and HER stability test are almost identical to that of the fresh sample, meaning no composition change of Ni and Fe. Apparently, the peaks for the high-resolution XPS spectrum of Cu 2p (Fig. S17c, ESI†) become stronger after the OER stability test, and the two satellite peaks confirm the existence of CuO,[63] indicating the oxidation of Cu to CuO. However, the EDS comparisons between before and after the OER stability test (Fig. S18, ESI†) show that the content of O just increases from 31.9% to 35.7%, which indicates that the amount of oxidized Cu is very small. Additionally, the thinner NiFe LDH layer on Cu after the stability test also makes the signal of Cu stronger. Most importantly, this does not weaken the OER and HER activities of the Cu@NiFe LDH catalysts (Fig. 6f), since the 3D core–shell nanostructures and compositions are mostly maintained. Therefore, our 3D core–shell Cu@NiFe LDH nanoarchitectures are highly efficient and stable bifunctional catalysts toward overall water splitting. In addition, our facile method to fabricate this 3D core–shell Cu@NiFe LDH catalyst on Cu foam can be effectively scaled up from 2 cm^2 to a larger size with a uniform surface morphology (Fig. S19, ESI†), which meets the prerequisites for practical applications. Even though the 3D core–shell Cu@NiFe LDH

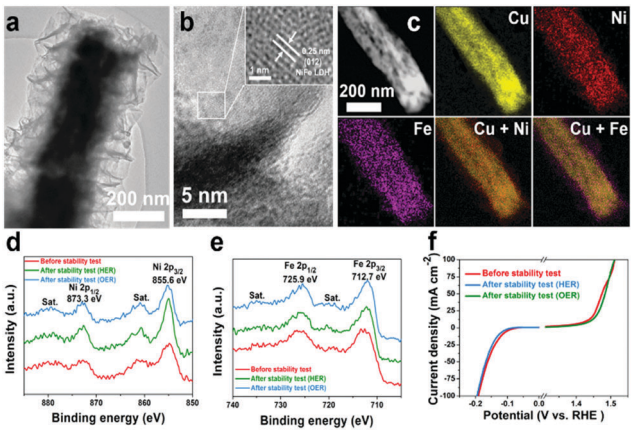

Fig. 6 Characterizations after the stability test. (a) TEM, (b) HRTEM, and (c) EDS elemental mapping of the Cu@NiFe LDH after the overall water splitting stability test (anode for OER). High-resolution XPS spectra of (d) Ni 2p and (e) Fe 2p, and (f) polarization curves of Cu@NiFe LDH before and after the overall water splitting stability test.

catalysts are very good for the HER, the OER, and overall water splitting, there is still room for further improvement, which will be our focus for future work.

Conclusions

In summary, we have developed a facile and scalable approach to fabricate a self-standing 3D core–shell Cu@NiFe LDH electrocatalyst for highly efficient overall water splitting. The catalyst not only exhibits outstanding OER performance, especially for high current densities, but also decent HER performance in an alkaline electrolyte. Thus, we have achieved a current density of 10 mA cm^{-2} at a voltage of 1.54 V, and 100 mA cm^{-2} at 1.69 V with excellent durability for overall water splitting, which has significantly advanced the science and technology of large-scale water splitting by electrolysis.

Acknowledgements

The work performed at the University of Houston is funded by the US Department of Energy under Award Number DE-SC0010831, and that in China is supported by the China Scholarship Council, and the National Natural Science Foundation of China (No. 21377044 and 21573085).

References

1 Z. W. Seh, J. Kibsgaard, C. F. Dickens, I. Chorkendorff, J. K. Nørskov and T. F. Jaramillo, *Science*, 2017, **355**, 4998–5009.
2 H. Q. Zhou, F. Yu, Y. Huang, J. Y. Sun, Z. Zhu, R. J. Nielsen, R. He, J. M. Bao, W. A. Goddard III, S. Chen and Z. F. Ren, *Nat. Commun.*, 2016, **7**, 12765–12771.
3 C. Tang, R. Zhang, W. Lu, Z. Wang, D. Liu, S. Hao, G. Du, A. M. Asiri and X. Sun, *Angew. Chem.*, 2017, **129**, 860–864.
4 H. Duan, D. Li, Y. Tang, Y. He, J. s. fang, R. Wang, H. Lv, P. P. Lopes, A. P. Paulikas and H. Li, *J. Am. Chem. Soc.*, 2017, **139**, 5494–5502.
5 M. G. Walter, E. L. Warren, J. R. McKone, S. W. Boettcher, Q. Mi, E. A. Santori and N. S. Lewis, *Chem. Rev.*, 2010, **110**, 6446–6473.
6 J. Yang, X. Wang, B. Li, L. Ma, L. Shi, Y. Xiong and H. Xu, *Adv. Funct. Mater.*, 2017, **27**, 1606497.
7 D. Li, H. Baydoun, B. Kulikowski and S. L. Brock, *Chem. Mater.*, 2017, **29**, 3048–3054.
8 Z. Pei, H. Li, Y. Huang, Q. Xue, Y. Huang, M. Zhu, Z. Wang and C. Zhi, *Energy Environ. Sci.*, 2017, **10**, 742–749.
9 K. Fan, Y. Ji, H. Zou, J. Zhang, B. Zhu, H. Chen, Q. Daniel, Y. Luo, J. Yu and L. Sun, *Angew. Chem., Int. Ed.*, 2017, **56**, 3289–3293.
10 Y. Zheng, Y. Jiao, Y. Zhu, Q. Cai, A. Vasileff, L. H. Li, Y. Han, Y. Chen and S. Z. Qiao, *J. Am. Chem. Soc.*, 2017, **139**, 3336–3339.
11 H. Liang, A. N. Gandi, C. Xia, M. N. Hedhili, D. H. Anjum, U. Schwingenschlögl and H. N. Alshareef, *ACS Energy Lett.*, 2017, **2**, 1035–1042.
12 B. Konkena, J. Masa, A. J. Botz, I. Sinev, W. Xia, J. R. Koßmann, R. Drautz, M. Muhler and W. Schuhmann, *ACS Catal.*, 2016, **7**, 229–237.
13 Y. Hou, M. Qiu, T. Zhang, J. Ma, S. Liu, X. Zhuang, C. Yuan and X. Feng, *Adv. Mater.*, 2017, **29**, 1604480.
14 S. Zhao, R. Jin, H. Abroshan, C. Zeng, H. Zhang, S. D. House, E. Gottlieb, H. J. Kim, J. C. Yang and R. Jin, *J. Am. Chem. Soc.*, 2017, **139**, 1077–1080.
15 T. Y. Ma, J. Ran, S. Dai, M. Jaroniec and S. Z. Qiao, *Angew. Chem., Int. Ed.*, 2015, **54**, 4646–4650.
16 B. Zhang, X. Zheng, O. Voznyy, R. Comin, M. Bajdich, M. García-Melchor, L. Han, J. Xu, M. Liu and L. Zheng, *Science*, 2016, **352**, 333–337.
17 S. H. Bae, J. E. Kim, H. Randriamahazaka, S. Y. Moon, J. Y. Park and I. K. Oh, *Adv. Energy Mater.*, 2017, **7**, 1601492.
18 Z. Pu, Y. Luo, A. M. Asiri and X. Sun, *ACS Appl. Mater. Interfaces*, 2016, **8**, 4718–4723.
19 S. Zhang, B. Chowdari, Z. Wen, J. Jin and J. Yang, *ACS Nano*, 2015, **9**, 12464–12472.
20 J. M. Woods, Y. Jung, Y. Xie, W. Liu, Y. Liu, H. Wang and J. J. Cha, *ACS Nano*, 2016, **10**, 2004–2009.
21 Y. J. Yuan, Z. J. Ye, H. W. Lu, B. Hu, Y. H. Li, D. Q. Chen, J. S. Zhong, Z. T. Yu and Z. G. Zou, *ACS Catal.*, 2015, **6**, 532–541.
22 W. Chen, T. Wang, J. Xue, S. Li, Z. Wang and S. Sun, *Small*, 2017, **13**, 1602420.
23 R. Zhang, M. Shao, S. Xu, F. Ning, L. Zhou and M. Wei, *Nano Energy*, 2017, **33**, 21–28.
24 Z. Li, M. Shao, H. An, Z. Wang, S. Xu, M. Wei, D. G. Evans and X. Duan, *Chem. Sci.*, 2015, **6**, 6624–6631.
25 Y. Hou, M. R. Lohe, J. Zhang, S. Liu, X. Zhuang and X. Feng, *Energy Environ. Sci.*, 2016, **9**, 478–483.
26 Z. Wang, S. Zeng, W. Liu, X.-W. Wang, Q. Li, Z. Zhao and F. Geng, *ACS Appl. Mater. Interfaces*, 2017, **9**, 1488–1495.
27 J. Liu, J. Wang, B. Zhang, Y. Ruan, L. Lv, X. Ji, K. Xu, L. Miao and J. Jiang, *ACS Appl. Mater. Interfaces*, 2017, **9**, 15364–15372.
28 R. D. Smith, M. S. Prévot, R. D. Fagan, Z. Zhang, P. A. Sedach, M. K. J. Siu, S. Trudel and C. P. Berlinguette, *Science*, 2013, **340**, 60–63.
29 X. Lu and C. Zhao, *Nat. Commun.*, 2015, **6**, 7616–7622.
30 H. Zhou, F. Yu, J. Sun, H. Zhu, I. K. Mishra, S. Chen and Z. Ren, *Nano Lett.*, 2016, **16**, 7604–7609.
31 C. Liu, L. Wang, Y. Tang, S. Luo, Y. Liu, S. Zhang, Y. Zeng and Y. Xu, *Appl. Catal., B*, 2015, **164**, 1–9.
32 Y. Jia, L. Zhang, G. Gao, H. Chen, B. Wang, J. Zhou, M. T. Soo, M. Hong, X. Yan and G. Qian, *Adv. Mater.*, 2017, **29**, 1700017.
33 J. Wang, H. X. Zhong, Z. L. Wang, F. L. Meng and X. B. Zhang, *ACS Nano*, 2016, **10**, 2342–2348.
34 C. A. Zhou, X. Xia, Y. Wang, Y. Zhong, Z. Yao, X. Wang and J. Tu, *J. Mater. Chem. A*, 2017, **5**, 1394–1399.
35 J. Wang, Q. Zhang, X. Li, D. Xu, Z. Wang, H. Guo and K. Zhang, *Nano Energy*, 2014, **6**, 19–26.
36 Y. Liu, X. Shang, W.-K. Gao, B. Dong, X. Li, X. Li, J. Zhao, Y. Chai, Y. Liu and C. Liu, *J. Mater. Chem. A*, 2017, **5**, 2885–2896.

37 J. X. Feng, H. Xu, Y. T. Dong, S. H. Ye, Y. X. Tong and G. R. Li, *Angew. Chem.*, 2016, **128**, 3758–3762.
38 F. Song and X. Hu, *Nat. Commun.*, 2014, **5**, 5477–5485.
39 Z. Li, M. Shao, L. Zhou, R. Zhang, C. Zhang, J. Han, M. Wei, D. G. Evans and X. Duan, *Nano Energy*, 2016, **20**, 294–304.
40 X. Han, C. Yu, J. Yang, C. Zhao, H. Huang, Z. Liu, P. M. Ajayan and J. Qiu, *Adv. Mater. Interfaces*, 2016, **3**, 1500782.
41 C. Xia, Q. Jiang, C. Zhao, M. N. Hedhili and H. N. Alshareef, *Adv. Mater.*, 2016, **28**, 77–85.
42 M. Gong, Y. Li, H. Wang, Y. Liang, J. Z. Wu, J. Zhou, J. Wang, T. Regier, F. Wei and H. Dai, *J. Am. Chem. Soc.*, 2013, **135**, 8452–8455.
43 F. Yu, H. Zhou, Z. Zhu, J. Sun, R. He, J. Bao, S. Chen and Z. Ren, *ACS Catal.*, 2017, **7**, 2052–2057.
44 X. Jia, Y. Zhao, G. Chen, L. Shang, R. Shi, X. Kang, G. I. Waterhouse, L. Z. Wu, C. H. Tung and T. Zhang, *Adv. Energy Mater.*, 2016, **6**, 1502585.
45 J. Duan, S. Chen, A. Vasileff and S. Z. Qiao, *ACS Nano*, 2016, **10**, 8738–8745.
46 Z. H. Xue, H. Su, Q. Y. Yu, B. Zhang, H. H. Wang, X. H. Li and J. S. Chen, *Adv. Energy Mater.*, 2017, 1602355.
47 D. Li, H. Baydoun, C. N. Verani and S. L. Brock, *J. Am. Chem. Soc.*, 2016, **138**, 4006–4009.
48 H. Q. Zhou, F. Yu, J. Y. Sun, R. He, S. Chen, C. W. Chua and Z. F. Ren, *Proc. Natl. Acad. Sci. U. S. A.*, 2017, **114**, 5607–5611.
49 Y. Wang, G. Zhang, W. Xu, P. Wan, Z. Lu, Y. Li and X. Sun, *ChemElectroChem*, 2014, **1**, 1138–1144.
50 M. Gao, C. Yang, Q. Zhang, J. Zeng, X. Li, Y. Hua, C. Xu and P. Dong, *J. Mater. Chem. A*, 2017, **5**, 5797–5805.
51 R. Chen, C. Yang, W. Cai, H.-Y. Wang, J. Miao, L. Zhang, S. Chen and B. Liu, *ACS Energy Lett.*, 2017, **2**, 1070–1075.
52 H. Zhou, Y. Wang, R. He, F. Yu, J. Sun, F. Wang, Y. Lan, Z. Ren and S. Chen, *Nano Energy*, 2016, **20**, 29–36.
53 T. Liu, X. Ma, D. Liu, S. Hao, G. Du, Y. Ma, A. M. Asiri, X. Sun and L. Chen, *ACS Catal.*, 2016, **7**, 98–102.
54 C. Tang, L. Gan, R. Zhang, W. Lu, X. Jiang, A. M. Asiri, X. Sun, J. Wang and L. Chen, *Nano Lett.*, 2016, **16**, 6617–6621.
55 D. Y. Chung, S. W. Jun, G. Yoon, H. Kim, J. M. Yoo, K. S. Lee, T. Kim, H. Shin, A. K. Sinha and S. G. Kwon, *J. Am. Chem. Soc.*, 2017, **139**, 6669–6674.
56 Y. T. Xu, X. Xiao, Z. M. Ye, S. Zhao, R. Shen, C. T. He, J. P. Zhang, Y. Li and X. M. Chen, *J. Am. Chem. Soc.*, 2017, **139**, 5285–5288.
57 Y. Jin, X. Yue, C. Shu, S. Huang and P. K. Shen, *J. Mater. Chem. A*, 2017, **5**, 2508–2513.
58 Y. Xu, W. Tu, B. Zhang, S. Yin, Y. Huang, M. Kraft and R. Xu, *Adv. Mater.*, 2017, **29**, 1605957.
59 H. Wang, H. W. Lee, Y. Deng, Z. Lu, P. C. Hsu, Y. Liu, D. Lin and Y. Cui, *Nat. Commun.*, 2015, **6**, 8261–8268.
60 C. Tang, N. Cheng, Z. Pu, W. Xing and X. Sun, *Angew. Chem., Int. Ed.*, 2015, **54**, 9351–9355.
61 Z. Y. Yu, Y. Duan, M. R. Gao, C. C. Lang, Y. R. Zheng and S. H. Yu, *Chem. Sci.*, 2017, **8**, 968–973.
62 J. Luo, J. H. Im, M. T. Mayer, M. Schreier, M. K. Nazeeruddin, N. G. Park, S. D. Tilley, H. J. Fan and M. Grätzel, *Science*, 2014, **345**, 1593–1596.
63 L. Yu, G. Li, X. Zhang, X. Ba, G. Shi, Y. Li, P. K. Wong, J. C. Yu and Y. Yu, *ACS Catal.*, 2016, **6**, 6444–6454.